Analysis of weak signal detection based on tri-stable system under Levy noise*

Li-Fang He(贺利芳)[1,2], Ying-Ying Cui(崔莹莹)[1,2,†], Tian-Qi Zhang(张天骐)[1,2], Gang Zhang(张刚)[1,2], and Ying Song(宋莹)[1,2]

[1] School of Communication, Chongqing University of Posts and Telecommunications, Chongqing 400065, China
[2] Key Laboratory of Signal and Information Processing of Chongqing, Chongqing 400065, China

(Received 21 January 2016; revised manuscript received 24 March 2016; published online 25 May 2016)

Stochastic resonance system is an effective method to extract weak signal. However, system output is directly influenced by system parameters. Aiming at this, the Levy noise is combined with a tri-stable stochastic resonance system. The average signal-to-noise ratio gain is regarded as an index to measure the stochastic resonance phenomenon. The characteristics of tri-stable stochastic resonance under Levy noise is analyzed in depth. First, the method of generating Levy noise, the effect of tri-stable system parameters on the potential function and corresponding potential force are presented in detail. Then, the effects of tri-stable system parameters w, a, b, and Levy noise intensity amplification factor D on the resonant output can be explored with different Levy noises. Finally, the tri-stable stochastic resonance system is applied to the bearing fault detection. Simulation results show that the stochastic resonance phenomenon can be induced by tuning the system parameters w, a, and b under different distributions of Levy noise, then the weak signal can be detected. The parameter intervals which can induce stochastic resonances are approximately equal. Moreover, by adjusting the intensity amplification factor D of Levy noise, the stochastic resonances can happen similarly. In bearing fault detection, the detection effect of the tri-stable stochastic resonance system is superior to the bistable stochastic resonance system.

Keywords: tri-stable system, Levy noise, stochastic resonance, bearing fault detection

PACS: 05.40.–a, 05.45.–a, 05.40.Fb, 02.60.Cb **DOI:** 10.1088/1674-1056/25/6/060501

1. Introduction

Stochastic resonance (SR) is a nonlinear phenomenon where the weak signal can be enhanced and the noise is weakened through the interaction among a nonlinear dynamic system, weak signal with small parameters and background noise.[1] Since SR was proposed by Benzi *et al.* in 1981,[2] SR has been widely used for detecting weak signals. Many new stochastic resonance models have been continually put forward, which were based on the classical one-dimensional Langevin equation. Lindner *et al.*[3] studied the nonlinear underdamped symmetrical monostable system and the way to improve the power spectrum of the signals with specific frequency by adjusting the noise. The SR was introduced for weak signal detection in bistable system in Refs. [4] and [5]. In recent years, the tri-stable systems have attracted more and more attention and many different tri-stable system models[6–8] were put forward from various angles. Arathi and Rajasekar explored the SR in a symmetric triple-well system with the different depths of the wells in Ref. [9]. The general tri-stable system model was defined and the dynamic characteristics of the tri-stable system were analyzed in depth in Ref. [10]. These findings were obtained basically in the Gaussian noise background, but the Gaussian noise is too idealistic to simulate the real noise which fluctuates drastically. As an important general noise model, Levy noise with long-tailed nature can simulate effectively the large-scale fluctuation so that it can reflect the random perturbation in the actual engineering more accurately. The parameter-induced stochastic resonance in an overdamped system under α stable noise was investigated by the random simulate method in Ref. [11]. The characteristics of power function type monostable SR under Levy noise were analyzed in Ref. [12]. The SR of asymmetric bistable system with α stable noise was also probed in Ref. [13].

The parameter-induced and noise-induced SR in a tri-stable system under Levy noise and their application researches in bearing fault diagnose have been so rarely studied until now. To solve the above problems, in this paper we study the characteristics of tri-stable SR under Levy noise on the basis of current researches about the tri-stable system. First, the tri-stable SR is presented by using self adaptive algorithms. Then the laws for the resonant output of tri-stable system governed by parameters w, a, b, and the intensity amplification factor D of Levy noise, are explored under Levy noise with different values of characteristic index α and symmetry parameter β. Finally, to study the validity and reliability of the tri-stable system, the bearing fault signal processing capability of tri-stable SR method and the classical bistable SR method

*Project supported by the National Natural Science Foundation of China (Grant No. 61371164), the Chongqing Municipal Distinguished Youth Foundation, China (Grant No. CSTC2011jjjq40002), and the Research Project of Chongqing Municipal Educational Commission, China (Grant No. KJ130524).

†Corresponding author. E-mail: 1294667224@qq.com

© 2016 Chinese Physical Society and IOP Publishing Ltd

are compared with each other and analyzed.

2. Models and methods

The Langevin equation of tri-stable system is considered as follows:

$$\frac{\mathrm{d}x}{\mathrm{d}t} = -\frac{\mathrm{d}U(x)}{\mathrm{d}x} + A\sin(2\pi f_0 t) + D\xi(t), \tag{1}$$

where $A\sin(2\pi f_0 t)$ is the system input signal to be measured, A is the amplitude of the input signal to be measured, f_0 is the frequency of the input signal to be measured, $D\xi(t)$ is the Levy noise with noise intensity amplification factor D, and $U(x)$ is the potential function of tri-stable system.

2.1. Tri-stable stochastic resonance system

$U(x)$ is the potential function of tri-stable system, and given as follows:

$$U(x) = \frac{1}{2}wx^2 - \frac{1}{4}bx^4 + \frac{1}{6}ax^6, \tag{2}$$

where w, a, and b are the structural parameters of tri-stable system, and these parameters meet such inequalities: $w, a, b > 0$ and $b^2 - 4aw > 0$. When there is no input signal, potential function contains three minima in the potential well and two maxima in the potential barrier which are given by

$$x_{\min} = 0, \pm\sqrt{\frac{b+\sqrt{b^2-4aw}}{2a}}, \tag{3}$$

$$x_{\max} = \pm\sqrt{\frac{b-\sqrt{b^2-4aw}}{2a}}. \tag{4}$$

Then, the depths of the wells can be obtained as

$$\Delta U_{\mathrm{L,R}} = \frac{1}{12a^2}(b^2-4aw)^{3/2}, \tag{5}$$

$$\Delta U_{\mathrm{M}} = \frac{1}{24a^2}[(b^2-4aw)^{3/2} + b(b^2-6aw)]. \tag{6}$$

As can be seen from formulas (5) and (6), the depths of the wells are associated with the parameters w, a, and b. In Fig. 1(a), the potential function $U(x)$ is even-symmetric about $x = 0$ and has three stable points and two potential barriers. The potential force $-U'(x)$ is odd-symmetric about $(0,0)$. It also shows that when an oscillating particle approaches to one side of the potential wall, the restoring potential force becomes large and makes the particle bounce back to the other side of the potential wall rapidly. Figure 1(b) shows the differences caused by w when $a = 1$ and $b = 4$, where the depths and widths of the lateral potential wells decrease with w increasing, on the contrary, the depths and widths of the middle potential wells increase with w increasing. Figure 1(c) shows the plots of potential force $-U'(x)$ versus position for different values of w when $a = 1$ and $b = 4$. The potential forces of the lateral potential wells first increase and then decrease.

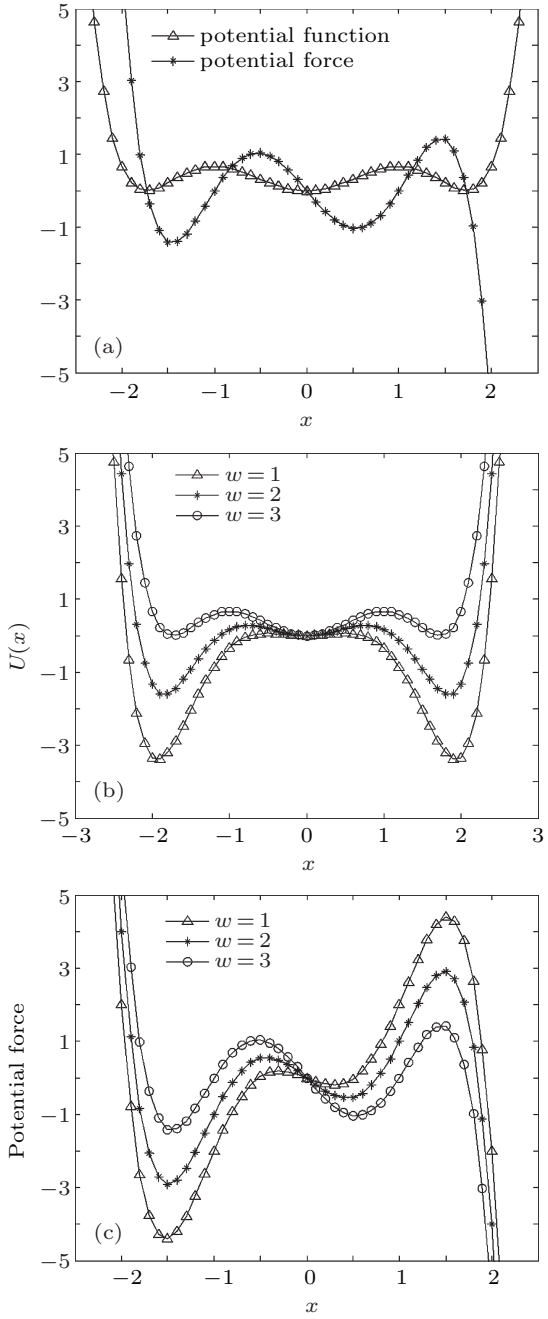


Fig. 1. Tristable potentials and potential forces (a); potentials (b) and potential forces for different values of w (c).

2.2. Characteristic function of Levy noise

Levy noise, also known as α stable noise,[14–16] was first proposed by Lindburg–Levy in studying the central limit theorem. The distribution of Levy noise can be generally described by a characteristic function, which can be written as:

$$\varphi(t) = \begin{cases} \exp\left[-\sigma|t|\left(1 + \mathrm{i}\beta\dfrac{2}{\pi}\mathrm{sign}(t)\log|t|\right) + \mathrm{i}\mu t\right], \\ \qquad \alpha = 1, \\ \exp\left[-\sigma^{\alpha}|t|^{\alpha}\left(1 - \mathrm{i}\beta\,\mathrm{sign}(t)\tan\left(\dfrac{\pi\alpha}{2}\right)\right) + \mathrm{i}\mu t\right], \\ \qquad \alpha \neq 1. \end{cases} \tag{7}$$

As shown in Eq. (7), the stable distribution of Levy

noise is related only to parameters α, β, σ, and μ. The α ($\alpha \in (0,2]$) denotes the characteristic index, which can affect the trailing and pulse characteristic of Levy noise. With the parameter α increasing, the tailing characteristics strengthen, while the pulse characteristics decrease. The Levy distribution will degenerate into the Gaussian distribution with $\alpha = 2$ and the Cauchy distribution with $\alpha = 1$. The β ($\beta \in [-1,1]$) is the skewness parameter which can determine the symmetry of the Levy distribution. The Levy stable distribution is symmetric about $\beta = 0$; The Levy stable distribution shows right-skewed with $\beta < 0$ and left-skewed with $\beta > 0$. σ ($\sigma \in [0,+\infty)$) is scale coefficient, also known as deviation or dispersion coefficient, which can measure the dispersion of the Levy distribution; μ ($\mu \in (-\infty,+\infty)$) is the mean parameter, which shows the center of distribution.

2.3. Method of generating Levy noise

Suppose that X is random variable which meets a Levy distribution,[17] and then it can be structured by Chambers–Mallows–Stuck (CMS) algorithm,[18,19] and shown as follows:

For $\alpha \neq 1$

$$X = D_{\alpha,\beta,\sigma}\frac{\sin(\alpha(V+C_{\alpha,\beta}))}{(\cos(V))^{1/\alpha}} \times \left[\frac{\cos(V-\alpha(V+C_{\alpha,\beta}))}{W}\right]^{(1-\alpha)/\alpha} + \mu, \quad (8)$$

where

$$C_{\alpha,\beta} = \frac{\arctan(\beta\tan(\pi\alpha/2))}{\alpha},$$

$$D_{\alpha,\beta,\sigma} = \sigma[\cos(\arctan(\beta\tan(\pi\alpha/2)))]^{-1/\alpha}. \quad (9)$$

For $\alpha = 1$

$$X = \frac{2\sigma}{\pi}\left[\left(\frac{\pi}{2}+\beta V\right)\tan V - \beta\ln\left(\frac{(\pi/2)W\cos V}{\pi/2+\beta V}\right)\right] + \mu, \quad (10)$$

where the random variable V is uniformly distributed in the interval $(-\pi/2,\pi/2)$ and W is exponentially distributed with a unit mean, and V and W are statistically independent. The Levy noises under different values of characteristic index α are plotted in Fig. 2, showing that the smaller the α value, the more pulse peaks the Levy noise contains, and that the amplitudes of these pulses are far greater than other sample average amplitudes in the sequence. The pulse characteristic of Levy noise gradually diminishes with α increasing. In Fig. 2(d), the pulse peak vanishes and the Levy distribution degenerates into the Gaussian distribution with $\alpha = 2$.

The fourth order Runge–Kutta method and CMS algorithm are combined to solve Eq. (1) in this paper, which can be defined as

$$x(n+1) = x(n) + \frac{1}{6}(k_1+2k_2+2k_3+k_4) + h^{1/\alpha}\eta(n), \quad (11)$$

in which

$$k_1 = h\left[-wx(n) + bx^3(n) - ax^5(n) + s(n)\right],$$

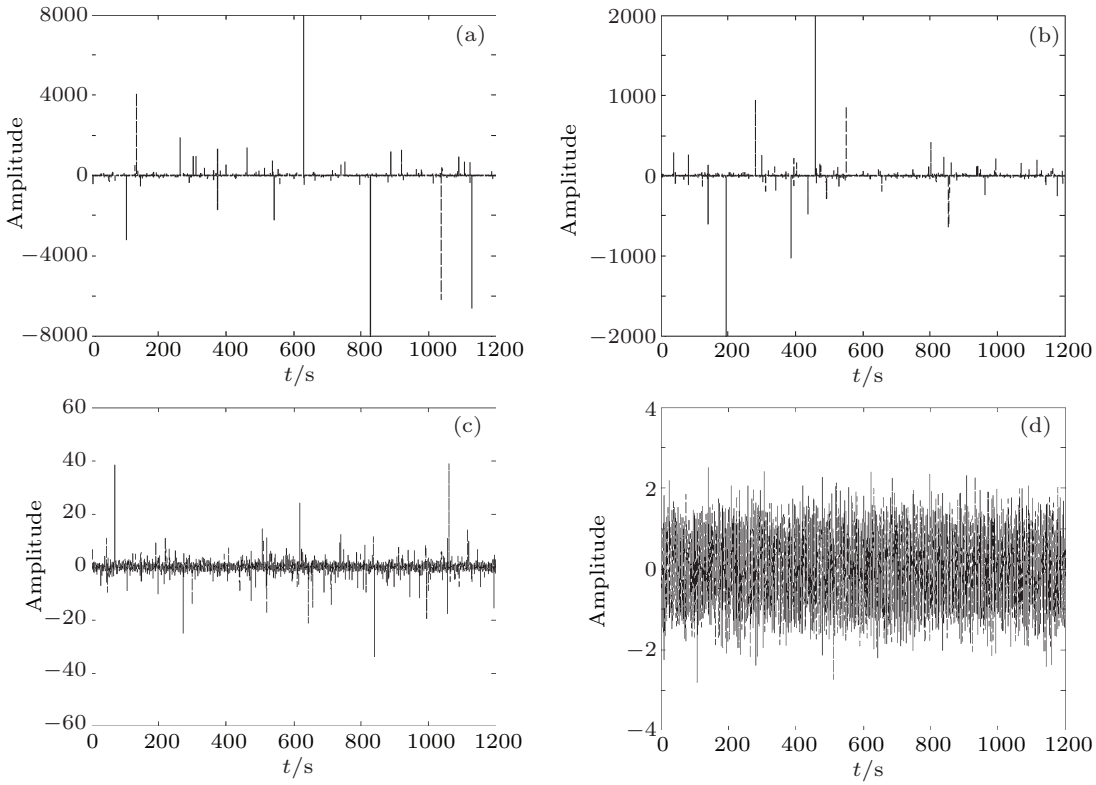


Fig. 2. Levy noises for characteristic index $\alpha = 0.8$ (a), 1.0 (b), 1.6 (c), and 2.0 (d), with $\beta = 0$, $\sigma = 1$, $\mu = 0$.

$$k_2 = h\left[-w\left(x(n)+\frac{k_1}{2}\right)+b\left(x(n)+\frac{k_1}{2}\right)^3 - a\left(x(n)+\frac{k_1}{2}\right)^5 + s(n)\right],$$

$$k_3 = h\left[-w\left(x(n)+\frac{k_2}{2}\right)+b\left(x(n)+\frac{k_2}{2}\right)^3 - a\left(x(n)+\frac{k_2}{2}\right)^5 + s(n+1)\right],$$

$$k_4 = h\left[-w\left(x(n)+k_3\right)+b\left(x(n)+k_3\right)^3 - a\left(x(n)+k_3\right)^5 + s(n+1)\right],$$

where $x(n)$ is the n-th sample value of the input signal, $s(n)$ is the n-th sample value of the output signal, $\eta(n)$ is the n-th sample value of Levy noise and h is the sampling interval. The smaller the characteristic index, the larger the amplitude of pulse is, and the jump tracks of oscillating particle may tend towards infinity. Aiming at this problem, the system output $x(t)$ is truncated,[20–22] and then the system output is written as $x(t) = \text{sign}(x(t)) \times 5$ when $|x(t)| > 5$.

3. Performance index

So far, there are varieties of indexes to measure the SR phenomenon, such as the amplification coefficients of power spectral, residence time distribution, SNR gain, etc. Among them, the SNR gain[23] reflects the effect of SR most visually, so the SNR gain is chosen in this paper as the index which is described as

$$\text{SNRGAIN} = \frac{S_{\text{out}}(f_0)/\xi_{\text{out}}(f_0)}{S_{\text{in}}(f_0)/\xi_{\text{in}}(f_0)}, \tag{12}$$

where $S_{\text{in}}(f_0)$ and $S_{\text{out}}(f_0)$ are the input and output signal power of SR system respectively, $\xi_{\text{in}}(f_0)$ and $\xi_{\text{out}}(f_0)$ are the input and output noise power of SR system respectively. Because of the high randomness of Levy noise, the SNR gain is not fixed in each simulation. To ensure statistical accuracy, the average SNR gain MR values in all the figures below are obtained as mean values of 100 independent simulations for the given parameter sets. MR is defined as

$$\text{MR} = \frac{1}{n}\sum_{j=1}^{n}\text{SNRGAIN}_j, \tag{13}$$

where MR is the average SNR gain, n is the simulation time, SNRGAIN_j denotes the SNR gain of the j-th system simulation.

4. Tri-stable stochastic resonance driven by Levy noise

When the input signal to be tested is $s(t) = A\sin(2\pi f_0 t)$ where $A = 0.5$ and $f_0 = 0.05$. The parameters of Levy noise distribution are set to be $\alpha = 1$, $\beta = 0$, $\sigma = 1$, $\mu = 0$, and $D = 0.3$. MR is chosen as the measure index. For each experiment, the sampling frequency is $f_s = 50$ Hz and the sampling number is $N = 10^4$. When system parameter is fixed to be $b = 2$, the optimal parameter pair (w, a) is discovered by using adaptive algorithms in Fig. 3(a). Figure 3(a) shows

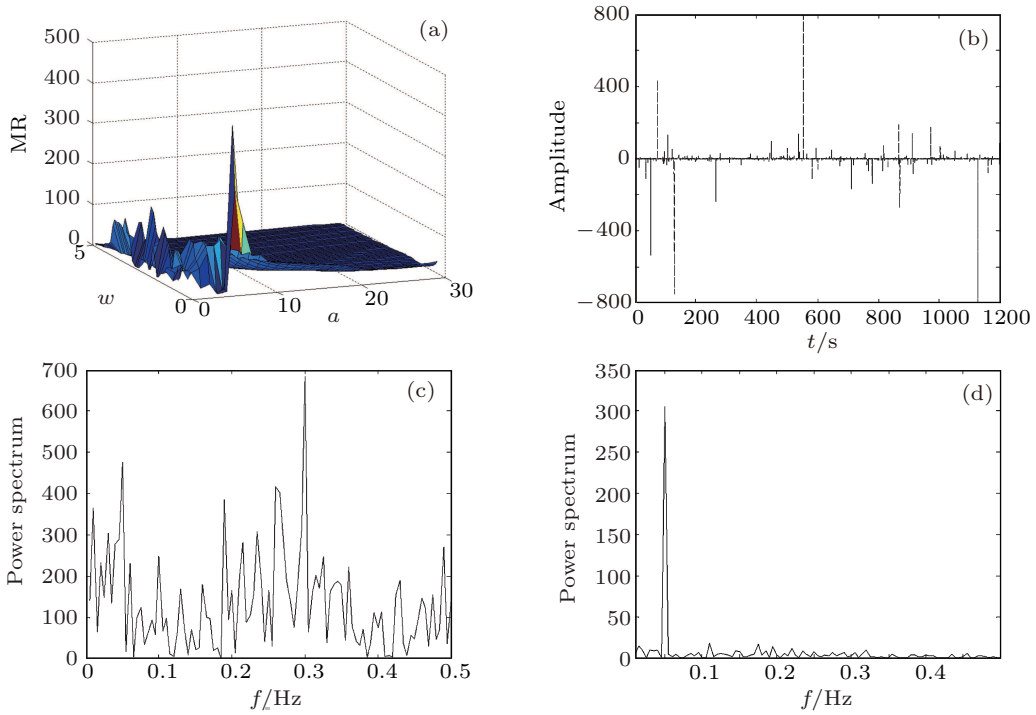


Fig. 3. (color online) (a) Three-dimensional diagram of adaptive SR, (b) the time domain diagram of noisy signal, and (c) the power spectrum diagram of noisy signal, and (d) the power spectrum diagram of output signal, for SR of a tristable system.

that the highest spectral peak is located at (2, 0.5), so the optimal system pair is $w = 2$, $a = 0.5$, and $b = 2$. Figure 3(b) shows the time domain diagram of noisy signal which contains the Levy noise and sinusoidal signal. Figure 3(c) is the power spectrum diagram of noisy signal. In Figs. 3(b) and 3(c), the input signal to be measured is completely submerged by Levy noise, so the frequency of the input signal cannot be identified. Figure 3(d) shows the power spectrum of the output signal through the tri-stable SR system. There is a peak at $f_0 = 0.05$ Hz located at the frequency of the measured signal. The conclusion can be obtained through the above analysis: by changing the system parameters and selecting the optimal parameter pair, the tri-stable system, Levy noise and the weak periodic signal can generate SR, and then the weak periodic signal can be detected.

Next, the laws for the resonant output of tri-stable system, governed by parameters w, a, and b and the intensity amplification factor D of Levy noise are explored under different values of characteristic index α and symmetry parameter β of Levy noise.

4.1. Stochastic resonances under different values of characteristic index α

4.1.1. Influences of system parameters on MR for different values of α

The input signal to be tested and the sampling frequency are consistent with the above results. The values of characteristic index α are 1.6, 1.0, and 0.8 respectively, other parameters are set to be $\beta = 0$, $\sigma = 1$, $\mu = 0$, and $D = 0.3$. For the parameters $a = 0.5$ and $b = 2$, the influence of the parameter w on MR is shown in Fig. 4. In Fig. 5, the influence of the parameter a on MR with $w = 2$, $b = 2$ is shown. For $a = 0.5$ and $w = 2$, the curve of MR versus parameter b is shown in Fig. 6.

Figure 4(a) shows that with the increase of parameter w, the curves of MR first increase and then decrease for different values of α. For $\alpha = 0.8$, the curve shows the double peaks, which means the resonances in the signal potential well and between the lateral potential wells are coexistent at this moment. MR curve shows that there is a smaller peak which is produced by the resonance in the middle potential well, and a bigger peak which is caused by the resonance between the lateral potential wells. Figure 4(b) shows the influence of the parameter w on MR for $\alpha > 1$. When $w \in (0, 1.81]$, MR is very small, which demonstrates that the system cannot produce SR. When $w \in (1.81, 5]$, there is a formant and the resonance peak interval is approximately the same. In Fig. 4(c), the curve of MR first increases and then decreases for $\alpha < 1$. Compared with Fig. 4(b), MR for $\alpha < 1$ is greater than MR for $\alpha > 1$ as a whole, which further validates the fact that the smaller the characteristic index of Levy noise, the stronger the pulse characteristics are.

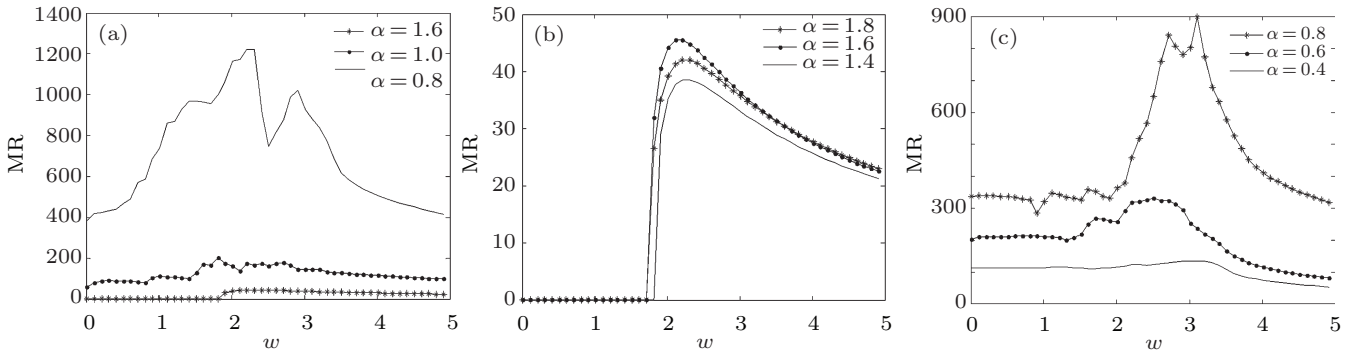


Fig. 4. Variations of MR with w for (a) different values of α, (b) $\alpha > 1$, and (c) $\alpha < 1$, respectively.

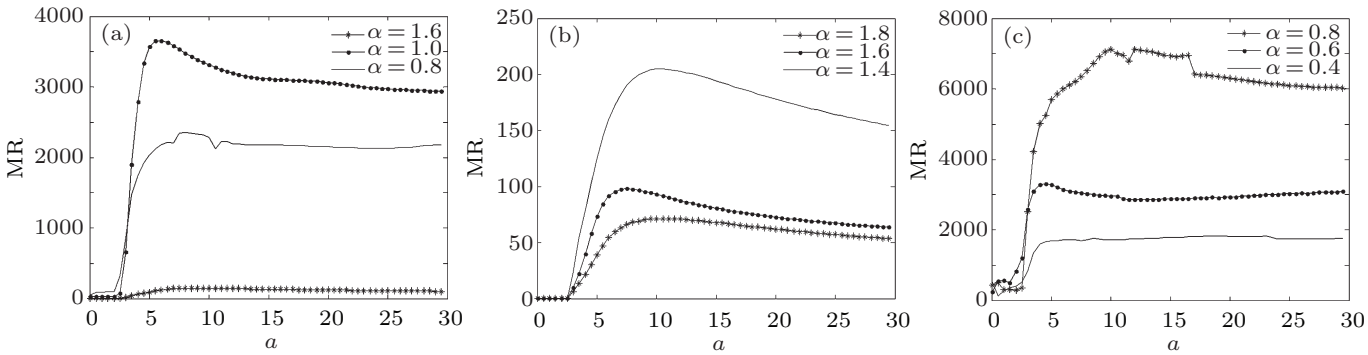


Fig. 5. Variations of MR with a for (a) different α values, (b) $\alpha > 1$, and (c) $\alpha < 1$, respectively.

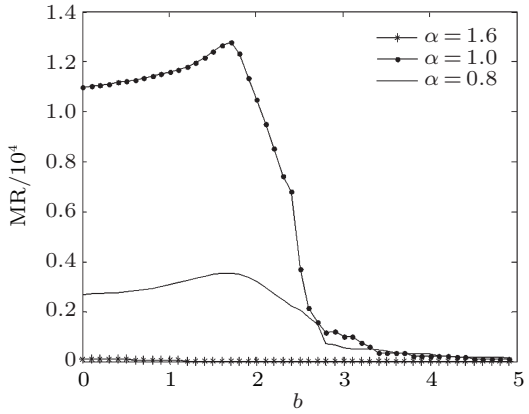


Fig. 6. Variations of MR with b for different values of α.

In Fig. 5(a), with the increase of parameter a, the curves of MR first increase and then decrease for different values of α. That is to say, there is the optimal system parameter a which can transfer more noise energy into useful signals to produce SR. Figure 5(b) shows the curves of MR for $\alpha > 1$, showing that MR curves first increase and then decrease to their corresponding certain value. MR for $\alpha = 1$ is greater than MR for $\alpha \neq 1$, and the smaller the characteristic index α, the bigger the MR. From Fig. 5(c), the characteristic index α becomes bigger with MR increasing when $\alpha < 1$.

As shown in Fig. 6, with the increase of parameter b, MR curves first increase and then decrease, and finally tend to 0 for different values of α. Also, MR curve for $\alpha = 1$ is greater than that when $\alpha \neq 1$. From the above analysis, it can be known that the parameter b has a significant impact on the features of SR.

4.1.2. Influence of intensity amplification factor of Levy noise D on MR for different values of α

The input signal to be tested and the sampling frequency are consistent with the above results and the values of characteristic index α are 1.8, 1.4, 1.0, 0.8, and 0.6 respectively. Other parameters are set to be $\beta = 0$, $\sigma = 1$ and $\mu = 0$. For parameters $a = 0.5$, $w = 2$ and $b = 2$, the influence of the intensity amplification factor D on MR is shown in Fig. 7. With D increasing, the curves of MR fluctuate and multiple maxima appear. It is shown that there is an optimal noise intensity, which induces better SR in the system. The maximum of MR for $\alpha = 1$ is significantly greater than the maximum of MR for $\alpha \neq 1$.

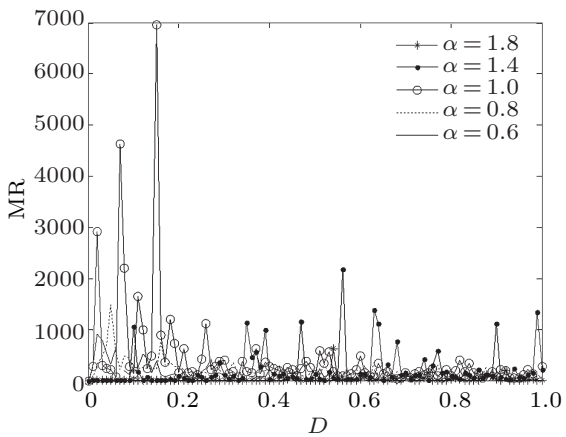


Fig. 7. Variations of MR with D for different values of α.

4.2. Stochastic resonances for different values of skewness parameter β

4.2.1. Influences of system parameters on MR for different values of β

The input signal to be tested and the sampling frequency are consistent with the above results. The skewness parameters take $\beta = -1$, $\beta = 0$ and $\beta = 1$, other parameters are set to be $\alpha = 1$, $\sigma = 1$, $\mu = 0$, and $D = 0.3$. For parameters $a = 0.5$ and $b = 2$, the influences of the system parameter w on MR for different values of β are shown in Fig. 8. For parameters $a = 0.5$ and $w = 2$, the influences of the system parameter b on MR for different values of β are shown in Fig. 9. For parameters $b = 2$ and $w = 2$, the influences of the system parameters a on MR for different values of β are shown in Fig. 10.

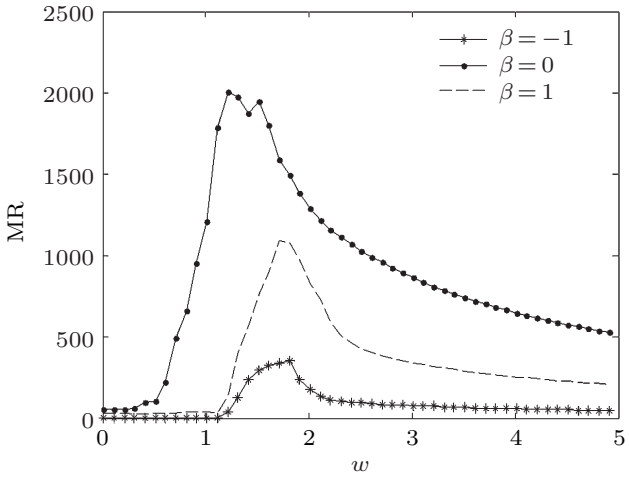


Fig. 8. Variations of MR with w for different values of β.

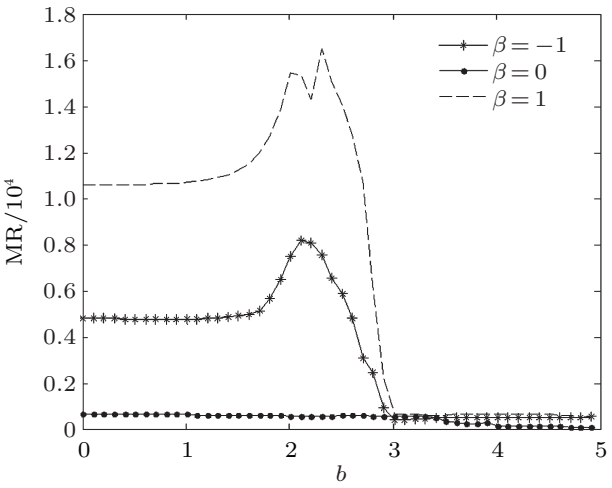


Fig. 9. Variations of MR with b for different values of β.

In Fig. 8, with w increasing, MR curves first increase and then decrease for different values of β, which indicates that there is an optimal β inducing better SR in the system. It can also be seen that the parameter intervals inducing SR are approximately equal for $\beta = -1$ and $\beta = 1$. And MR for $\beta = 0$ is significantly greater than MR for $\beta \neq 0$. In Fig. 9, with b increasing, there are obvious resonance peaks for different values of β, and the positions which are in a range of 1.81–3, i.e., $b \in [1.81, 3]$, of the formant are roughly the same. Furthermore, MR for $\beta = 0$ is far less than MR for $\beta \neq 0$, which is exactly opposite to the scenario of the bistable system and the power function type of monostable system under Levy noise. The influences of the system parameter a on MR for different values of β are shown in Fig. 10. It can be seen that MR also first increases then decreases with a increasing and MR for $\beta \neq 0$ is much less than that for $\beta = 0$.

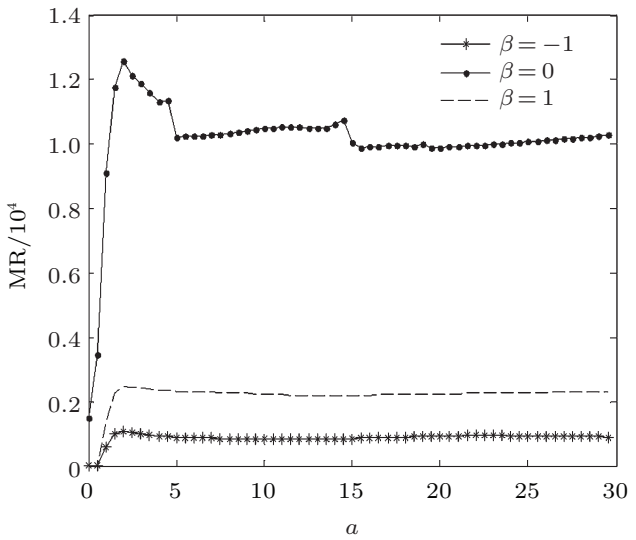


Fig. 10. Variations of MR with a for different values of β.

4.2.2. Influences of intensity amplification factor D on MR for different values of β

The input signal to be tested and the sampling frequency are consistent with the above results. It is assumed that $\beta = -1$, $\beta = 0$, and $\beta = 1$, other parameters are set to be $\alpha = 1$, $\sigma = 1$, and $\mu = 0$. For parameters $a = 0.5$, $w = 2$, and $b = 2$ in the simulation experiment, the variations of curves of MR with intensity amplification factor D are obtained for different values of β, which are demonstrated in Fig. 11. With D increasing, the curves of MR first increase and then decrease as a whole for different values of β. Furthermore, the parameter D intervals which produce better SR are basically concentrated in the same area, and MR for $\beta = 0$ is much greater than that for $\beta \neq 0$. The above analysis also shows that there is an optimal D to produce better SR.

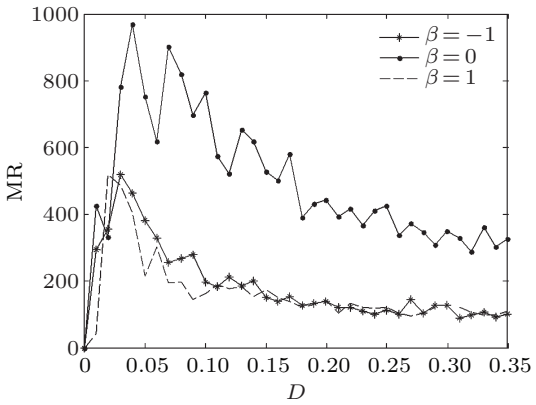


Fig. 11. Variations of MR with D for different values of β.

5. Engineering application

To further validate the applicability of the tri-stable system to the bearing fault signal detection in practice, the fault data of rolling element bearing in outer-raceway and inner-raceway are analyzed in the following respectively. The bearing fault data are cited from the Bearing Data Center in Case Western Reserve University (CWRU),[24,25] and the experimental equipment is shown in Fig. 12. The deep groove ball bearing with the type of 6205-2RS JEM SKF is chosen as a test object and its geometric parameters are provided in Table 1. The sampling frequency is $f_s = 12$ kHz, the shaft speed is 1796 r/min, the data length is 4000 and the bearing data are processed by twice sampling[26] whose compression ratio is $R = 2400$. The fault characteristic frequencies can be calculated theoretically based on the bearing type and the shaft/rotating speed as follows:[27]

$$f_{\mathrm{BPFI}} = \frac{n_{\mathrm{r}} f_{\mathrm{r}}}{2}\left(1 + \frac{D_1}{D_2}\cos\alpha\right), \tag{14}$$

$$f_{\mathrm{BPFO}} = \frac{n_{\mathrm{r}} f_{\mathrm{r}}}{2}\left(1 - \frac{D_1}{D_2}\cos\alpha\right), \tag{15}$$

where α is the bearing contact angle, n_{r} and f_{r} are the number of rolling elements and the rotating frequency of the shaft respectively, D_1 is the diameter of one rolling element, D_2 is the pitch diameter of the bearing. f_{BPFI} is the bearing characteristic frequency when the fault appears in inner raceway, f_{BPFO} is the bearing characteristic frequency when the fault appears in outer raceway.

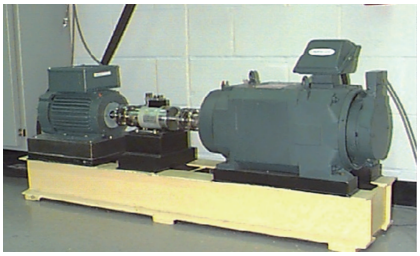


Fig. 12. (color online) Bearing test stand from CWRU.

Table 1. Geometric parameters of the test bearing. The unit 1 inch = 2.54 cm.

Inside Diameter (inches)	Outside Diameter (inches)	Thickness (inches)	Ball Diameter (inches)	Pitch Diameter (inches)	No. of rolling elements
0.9843	2.0472	0.5906	0.3126	1.537	9

5.1. Bearing outer raceway fault detection

According to Eq. (15), the bearing characteristic frequency when the fault appears at outer raceway is theoretically $f_{\mathrm{BPFO}} = 107.28$ Hz. Figures 13(a) and 13(b) show the original signal and its power spectrum. It can be seen that the average period of impulses is 0.01 s, which is larger than the period of the characteristic frequency ($1/f_{\mathrm{BPFO}} = 0.009$ s). It means that other fault impulses are so weak that they are submerged by the background noise. But, a resonance band can be clearly found in its power spectrum. Figures 13(c) and 13(d), figures 13(e) and 13(f) show the detection results of classical bistable SR model with $a = 1$, $b = 1$ and tri-stable SR model with $a = 4$, $b = 0.8$, $w = 0.032$ respectively. In Fig. 13(d), there is a maximum spectrum peak located at $f = 105$ Hz and it is 1.99. Similarly, there is a maximum spectrum located at $f = 105$ Hz in Fig.13(f), but the corresponding spectrum increases to 2.358. The error between the detected frequency and the theoretical frequency is $|f - f_{\mathrm{BPFO}}| = 2.28$ Hz, which is at an acceptable error level. The above analysis verifies the effectiveness of the tri-stable SR system in the bearing fault signal detection with outer-raceway defect, and the detection effect of tri-stable SR system is superior to the classical bistable SR system.

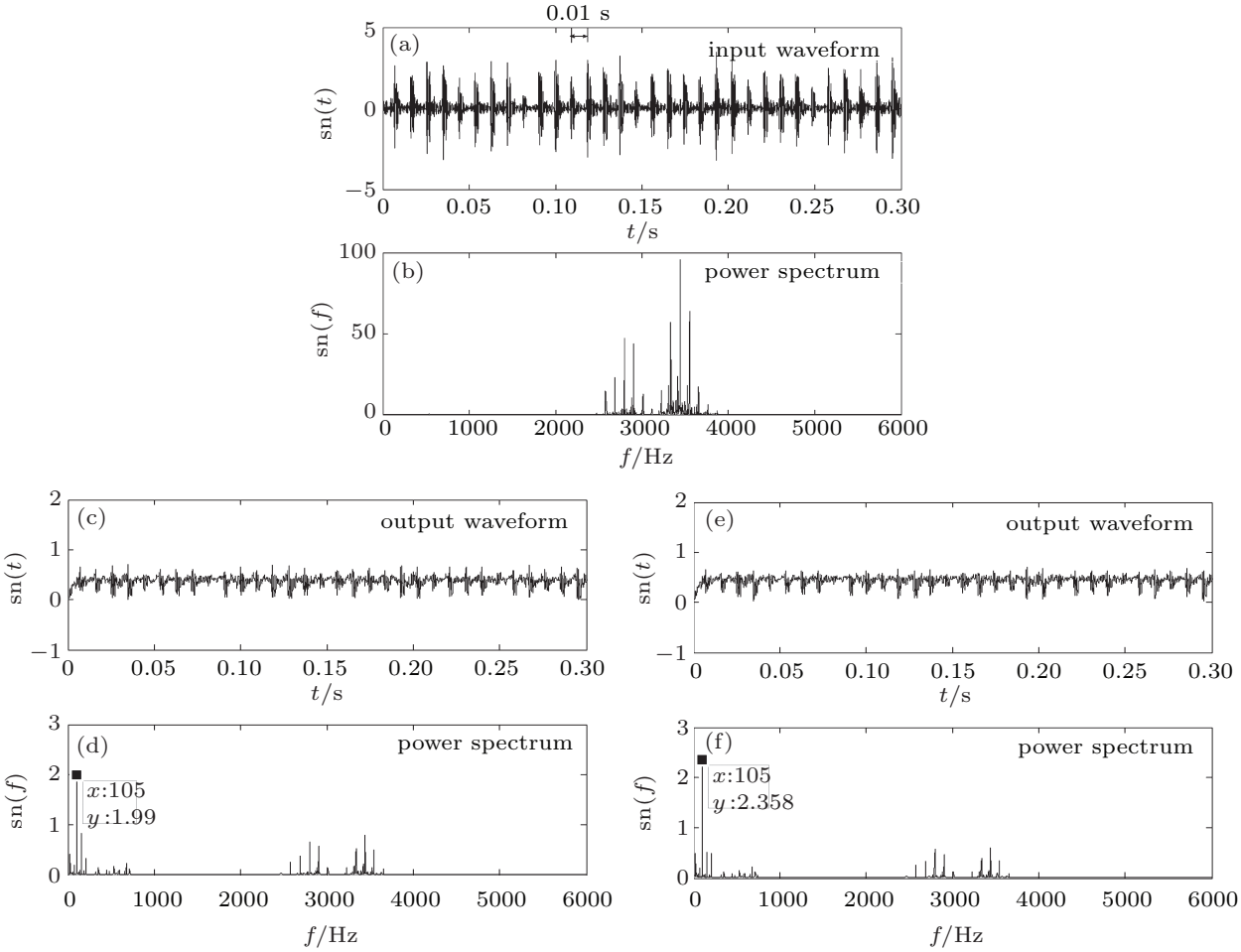


Fig. 13. Simulation results of the outer raceway defective signal detection, showing time domains and frequency domains of (a) and (b) the original fault signal, (c) and (d) the output signal after a bistable system, and (e) and (f) the output signal after a tri-stable system, respectively.

5.2. Bearing inner raceway fault detection

According to Eq. (14), the bearing characteristic frequency when the fault appears at inner raceway is theoretically $f_{\mathrm{BPFI}} = 162.11$ Hz. The original signal and its power spectrum are shown in Figs. 14(a) and 14(b), where the fault impulses are not obvious in the input waveform due to the strong noise. The output of classical bistable SR system and the output of the tri-stable system are shown in Figs. 14(c) and 14(d), and Figs. 14(e) and 14(f), respectively.

As shown in Figs. 14(c) and 14(d) with $a = 1$ and $b = 1$,

some of the high-frequency components are weakened and the target frequency is enhanced. There is a maximum spectral peak located at $f = 159$ Hz (the feature frequency within an acceptable error range) and its value is 0.778. It can be seen from Fig. 14(f) with $a = 0.01$, $b = 0.01$, and $w = 0.04$ that, the amplitude of $f = 159$ Hz rises to 1.462, that is, 1.88 times the amplitude in Fig. 14(d). Therefore it effectively shows that the fault appears at inner raceway and the detection effect of tri-stable SR system is superior to the classical bistable SR system.

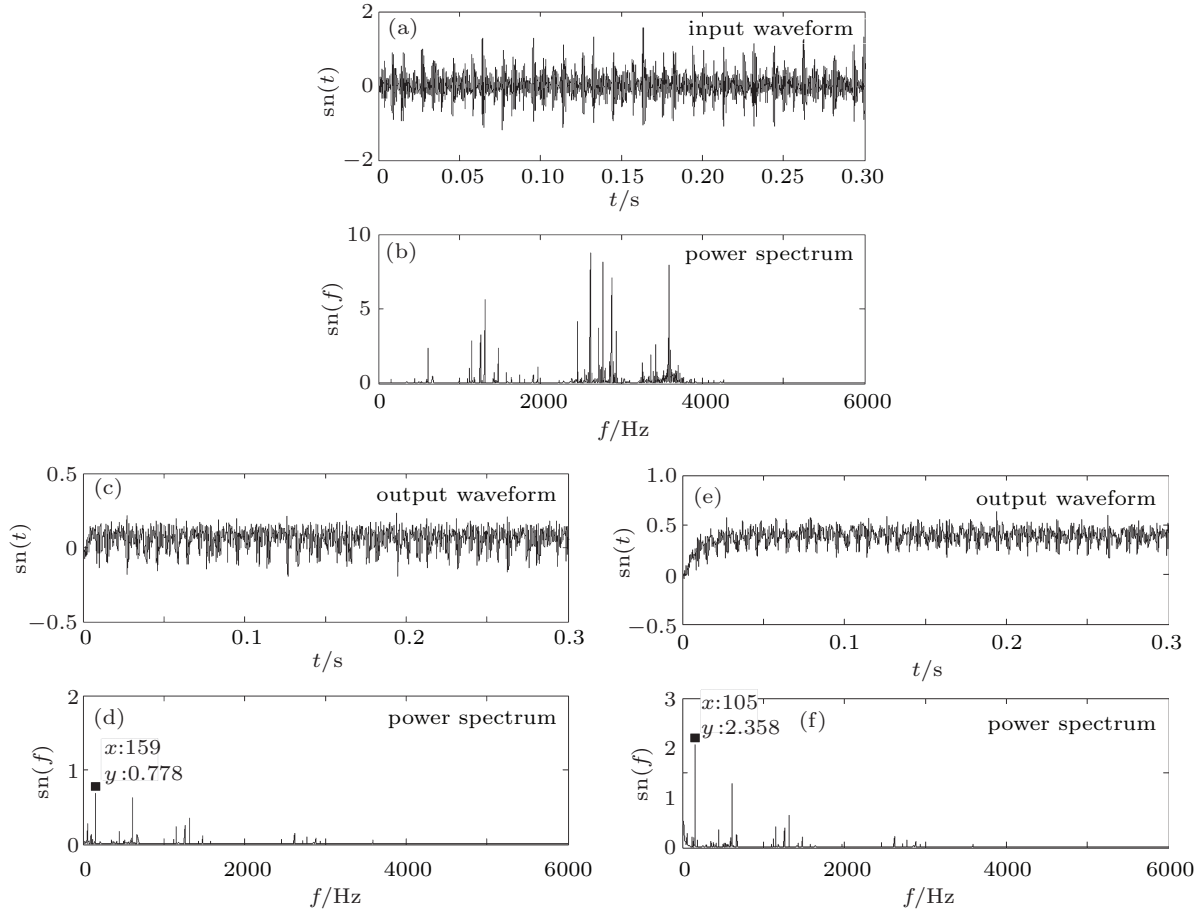


Fig. 14. Simulation results of the inner raceway defective signal detection, showing time domains and frequency domains of (a) and (b) the original fault signal, (c) and (d) output signal after a bistable system, and (e) and (f) output signal after a tri-stable system, respectively.

6. Conclusions

In this paper, we explore the tri-stable SR phenomenon induced by parameters and Levy noise, and apply the tri-stable SR to the bearing fault detection. From the results we can draw the following conclusions: (i) No matter whether it is under any different characteristic index α or symmetry parameter β of Levy noise, the SR can be induced by tuning parameters a, b, w, and the intensity amplification factor D of Levy noise. (ii) For a certain system parameter w (or a or b), MR first increases and then decreases for different values of characteristic index α, which explains that there exists an optimal system parameter producing better SR. For $\alpha = 1$, the resonance effect is best. Moreover, MR for $\alpha > 1$ is much less than MR for $\alpha < 1$. (iii) For a certain intensity amplification factor D, the curves of MR have multiple maxima for different values of characteristic index α. The resonance effect for $\alpha = 1$ precedes the resonance effect for $\alpha \neq 1$. (iv) For any system parameters w, a, and intensity amplification factor D, the system performance is best for $\beta = 0$, but as for the system parameter b, the resonance effect for $\beta \neq 0$ is much better than the resonance effect for $\beta = 0$. (v) In bearing fault signal detection, the detection effect of tri-stable SR system is superior to the classical bistable SR system.

References

[1] Li J M, Chen X F and He Z J 2013 *J. Sound Vib.* **332** 5999
[2] Benzi R, Sutera A and Vulpiani A 1981 *J. Phys. A: Math. Gen.* **14** L453
[3] Lindner J F, Breen B J, Wills M E, Bulsara A R and Ditto W L 2001 *Phys. Rev. E* **63** 175
[4] Wang K K and Liu X B 2014 *Chin. Phys. B* **23** 010502
[5] Liu H B, Wu D W, Dai C J and Mao H 2013 *Acta Electron Sin.* **41** 8 (in Chinese)
[6] Lu S L, He Q B, Zhang H B, Zhang S B and Kong F R 2013 *Rev. Sci. Instrum.* **84** 026110
[7] Ghosh P K, Bag B C and Ray D S 2007 *Phys. Rev. E* **75** 032101
[8] Zhang H Q, Xu Y, Xu W and Li X C 2012 *Chaos* **22** 043130
[9] Arathi S and Rajasekar S 2011 *Phys. Scr.* **84** 065011
[10] Lai Z H and Leng Y G 2015 *Acta Phys. Sin.* **64** 200503 (in Chinese)
[11] Zhang G L, Lv X L and Kang Y M 2012 *Acta Phys. Sin.* **61** 040501 (in Chinese)

[12] Zhang G, Hu T and Zhang T Q 2015 *Acta Phys. Sin.* **64** 220502 (in Chinese)
[13] Jiao S B, Yang R, Zhang Q and Xie G 2015 *Acta Phys. Sin.* **64** 020502 (in Chinese)
[14] Xu B H, Zeng L Z and Li J L 2007 *J. Sound Vib.* **303** 255
[15] Dybiec B and Gudowska-Nowak E 2006 *Acta Phys. Polo. B* **37** 1479
[16] Tang Y, Zou W, Lu J Q and Kurths J 2012 *Phys. Rev. E* **85** 046207
[17] Xu Y, Li Y G, Li J J, Feng J and Zhang H Q 2015 *J. Statist. Phys.* **158** 120
[18] Chambers J M 1976 *J. Am. Stat. Assoc.* **71** 340
[19] Weron A and Weron R 1995 *Lec. Notes Phys.* **457** 379
[20] Weron R 1996 *Statist. Prob. Lett.* **28** 165
[21] Zeng L Z and Xu B H 2010 *Physica A: Statistical Mechanics and its Applications* **22** 5128
[22] Jiao S B, Ren C, Huang W C and Liang Y M 2013 *Acta Phys. Sin.* **62** 210501 (in Chinese)
[23] Wan P, Li X C, Wang Y H and Zhan Y J 2011 *Acta Phys. Sin.* **60** 040502 (in Chinese)
[24] Lei Y G, Li N P, Lin J and Wang S Z 2013 *Sensors* **13** 16950
[25] He Q B, Wang X X and Zhou Q 2014 *Sensors* **14** 382
[26] Leng Y G and Wang T Y 2003 *Acta Phys. Sin.* **52** 2432 (in Chinese)
[27] Lu S L, He Q B and Kong F R 2015 *Digital Signal Processing* **36** 93